BIOCHEMISTRY
including biophysical chemistry & molecular biology
Article

Biochemistry **2009,** *48,* 4881–4894 4881
DOI: 10.1021/bi801738j

Factors Controlling the Reactivity of Hydrogen Sulfide with Hemeproteins[†]

Ruth Pietri,[‡] Ariel Lewis,[§] Ruth G. León,[∥] Gullermina Casabona,[⊥] Laurent Kiger,[@] Syun-Ru Yeh,[§] Sebastian Fernandez-Alberti,[⊥] Michael C. Marden,[@] Carmen L. Cadilla,[∥] and Juan López-Garriga*[,‡]

[‡]*Department of Chemistry, University of Puerto Rico, Mayagüez Campus, P.O. Box 9019, Mayagüez, Puerto Rico 00681-9019,* [§]*Department of Physiology and Biophysics, Albert Einstein College of Medicine, 1300 Morris Park Avenue, Bronx, New York 10461,* [∥]*Department of Biochemistry, School of Medicine, University of Puerto Rico, Medical Sciences Campus, P.O. Box 365067, San Juan, Puerto Rico 00936-5067,* [⊥]*Universidad Nacional de Quilmes, 1876 Bernal, Argentina, and* [@]*INSERM U779, University of Paris 11, Hôpital de Bicetre, 94275 Le Kremlin-Bicetre, France*

Received September 10, 2008; Revised Manuscript Received March 20, 2009

ABSTRACT: Hemoglobin I (HbI) from the clam *Lucina pectinata* is an intriguing hemeprotein that binds and transports H_2S to sulfide-oxidizing chemoautotrophic bacteria to maintain a symbiotic relationship and to protect the mollusk from H_2S toxicity. Single point mutations at E7, B10, and E11 were introduced into the HbI heme pocket to define the reactivity of sulfide with hemeproteins. The functional and structural properties of mutant and wild-type recombinant proteins were first evaluated using the well-known ferrous CO and O_2 derivatives. The effects of these mutations on the ferric environment were then studied in the metaquo and hydrogen sulfide derivatives. The results obtained with the ferrous HbI mutants show that all the E7 substitutions and the PheB10Tyr mutation influence directly CO and O_2 binding and stability while the B10 and E11 substitutions induce distal structural rearrangements that affect ligand entry and escape indirectly. For the metaquo−GlnE7His, −PheB10Val, −PheB10Leu, and −E11 variants, two individual distal structures are suggested, one of which is associated with H-bonding interactions between the E7 residues and the bound water. Similar H-bonding interactions are invoked for these HbI−H_2S mutant derivatives and the rHbI, altering in turn sulfide reactivity within these protein samples. This is evident in the resonance Raman spectra of these HbI−H_2S complexes, which show reduction of heme iron as judged by the appearance of the ν_4 oxidation state marker at 1356 cm^{-1}, indicative of heme−Fe^{II} species. This reduction process depends strongly on distal mutations showing faster reduction for those HbI mutants exhibiting the strongest H-bonding interactions. Overall, the results presented here show that (a) H_2S association is regulated by external kinetic barriers, (b) H_2S release is controlled by two competing reactions involving simple sulfide dissociation and heme reduction, (c) at high H_2S concentrations, reduction of the ferric center dominates, and (d) reduction of the heme is also enhanced in those HbI mutants having polar distal environments.

Hydrogen sulfide (H_2S) is a well-known poisonous gas whose cytotoxic effects have been studied for more than 300 years (*1*). Interestingly, it has been found recently that H_2S is produced in mammalian tissues and that, similar to nitric oxide (NO) and carbon monoxide (CO), it may function as a neuromodulator, neuroprotector, and/or smooth muscle relaxant/constrictor (*2*−*5*). Endogenous H_2S is produced at high concentrations in the brain (100 μM) by cystathionine β-synthase enzyme (CBS, EC 4.2.1.22), where it acts as neuromodulator and neuroprotector, and in the peripheral tissues by cystathionine α-lyase enzyme (CSE, EC 4.4.1.1), where it functions as a relaxant/constrictor. As a neuromodulator, H_2S enhances the activity of the *N*-methyl-D-aspartate (NMDA) receptor and activates Ca^{2+} channels regulating synaptic transmission in neurons. As a neuroprotector, H_2S enhances the activity of the enzyme responsible for producing glutathione, activates K^+_{ATP} and Cl^- channels, and acts against oxidative stress. The muscle relaxant activity of H_2S is believed to be dictated by mediation of K^+_{ATP} channels in the ileum, portal vein, and thoracic aorta tissues, while its vasoconstrictor action is believed to be in part through inhibition of eNOS activity (*2*−*5*).

As for NO and CO, there is not a single H_2S receptor responsible for all the biological activities found until now. In fact, it has been suggested that H_2S can bind to hemeproteins, inducing different responses that in turn modulate its cytotoxic and cytoprotective activities (*6*). For instance, H_2S reacts with mitochondrial cytochrome *c* oxidase in a concentration-dependent manner either to completely inhibit the enzyme, producing cytotoxic effects, or to reversibly modulate its activity, resulting in induction of a suspended animation-like state that can stimulate cytoprotective effects (*7*). In this regard, it has been

[†]This work was supported in part by funds from the National Science Foundation, Cellular Biology (Grant 0544250), and NIH-NIGMS/MBRS-SCORE S06GM08103-34, NCRR G12RR03051, P20RR016439, and NCMHD T37MD001477 and Inserm. R.P. thanks the Alfred P. Sloan (NACME) and CNY-PR AGEP for their fellowship support.

*To whom correspondence should be addressed. Telephone: (787) 265-5453. Fax: (787) 265-5476. E-mail: sonw@caribe.net.

 Published on Web 04/15/2009

observed that interaction of H_2S with the resting enzyme at low sulfide levels (at a 1:1 stoichiometry), instead of stimulating irreversible inhibition, reduces the heme a_3 cytochrome center in a reaction that results in the formation of a ferrous intermediate, uptake of O_2, and conversion to a low-spin ferric derivative (*8*, *9*). This low-spin form of the heme a_3 center is unable to bind oxygen, reducing its uptake and thereby downregulating cellular respiration. It is at this level of regulation that H_2S is suggested to exert protective effects in mammals (*6*, *7*). At a higher stoichiometry, however (3 mol of H_2S per mole of enzyme), the toxicity of H_2S becomes apparent by the reduction of the other metal centers with its concomitant ligation to the heme a_3 group, producing the final, nonfunctional enzyme (*7*−*10*).

On the other hand, reactions of H_2S with myoglobin and hemoglobin, in the presence of O_2, result in covalent modification of one of the pyrrole rings of the heme, generating the so-called sulfmyoglobin and sulfhemoglobin derivatives, respectively (*11*). These compounds are proposed to protect the cell from H_2S toxicity (*6*). Others have argued against a protective role of these sulfheme compounds, since they have been found in a number of human diseases involving poisoning with sulfide-containing drugs and not with H_2S itself (*12*, *13*). More recently, a study concerning the interaction of human neuroglobin with H_2S suggested that this ligand binds tightly to the protein heme active site and, as a consequence, can have cytoprotective effects in the brain when levels of H_2S increase (*14*).

Evidently, H_2S exerts different responses on hemeproteins and, consequently, the cell. Nevertheless, the factors controlling heme−H_2S interactions required to produce all these biological responses are still unknown. Understanding these factors is therefore crucial before exploiting the potential of H_2S in therapeutic interventions. Intriguingly, interactions of H_2S with hemeproteins have been recognized and studied for many years in marine invertebrate organisms that live in sulfide-rich environments (*15*). These organisms have evolved strategies for avoiding sulfide toxicity, including the binding and oxidation of H_2S by hemoglobins and symbiotic bacteria, respectively. In this context, the giant tubeworm *Riftia pachyptila*, which lives in deep sea hydrothermal vents, supplies O_2 and H_2S to the endosymbionts by binding both ligands simultaneously at two different sites on their extracellular hemoglobins (*13*, *15*). The bacteria living inside the tubeworm oxidize H_2S in the presence of O_2 and utilize this energy to synthesize organic nutrients for the invertebrate.

The clam *Lucina pectinata* is another interesting invertebrate that lives in sulfide-rich mangroves and is also characterized by the presence of symbiotic sulfide-oxidizing bacteria that need to be supplied with both H_2S and O_2 (*16*, *17*). The protein responsible for delivering H_2S to the bacteria is a hemeprotein called hemoglobin I (HbI). HbI is one of the few known H_2S carriers in organisms that have been implicated in physiologically binding this molecule in the ferric heme−iron center to maintain the symbiotic relationship with the bacteria as well as to protect the clam from H_2S cytotoxicity. The affinity of hydrogen sulfide for ferric HbI is exceptionally high and is believed to be achieved through fast association ($k_{on} = 2.3 \times 10^5\ M^{-1}\ s^{-1}$) and very slow dissociation processes ($k_{off} = 0.22 \times 10^{-3}\ s^{-1}$). Structural studies of the HbI active site have shown that HbI has a glutamine (Gln) residue at the distal E7 position instead of the typical histidine (His) found in mammalian myoglobins and hemoglobins (*18*). In addition to GlnE7, HbI has phenylalanine residues (Phe) at the B10 and E11 distal positions, generating what is known as the "Phe cage". Figure 1 shows the peculiar amino acid composition

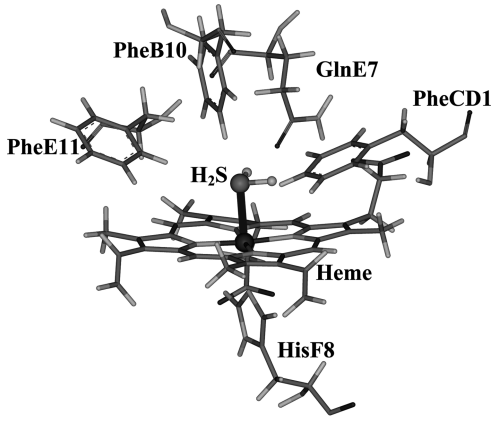

FIGURE 1: Representation of key residues in the heme pocket of HbI from *L. pectinata*, taken from ref *35*.

of the HbI distal ligand binding site, which has been suggested to be responsible for the high H_2S affinity. In contrast, the other two hemoglobins found in *L. pectinata* (HbII and HbIII) have a tyrosine at the B10 position, which prevents H_2S binding in these two hemeproteins (*19*−*21*). Indeed, spectroscopic studies of HbI with various ligands (*22*, *23*) have demonstrated a flexibility of the GlnE7 residue that controls ligand access to the HbI heme pocket, while hydrogen bonding and multipole interactions of this residue and the Phe cage have been thought to be involved in H_2S stability and release. Despite all these significant findings, a comprehensive understanding of H_2S binding, stability, and release to and from HbI has not been established. Thus, a study aimed at defining the role of the heme pocket amino acids in the kinetics and dynamics of H_2S binding and release to and from the heme active site of HbI and the structural aspects associated with these processes is necessary to unravel the relationship among the structure, function, and dynamics of the HbI−H_2S moiety. Furthermore, these results can provide an overall picture of the role of the heme distal structural environment in hemeprotein−H_2S interaction.

The functional aspects of many hemeproteins have been systematically examined by site-directed mutagenesis and kinetic analyses with various gaseous ligands (*24*, *25*). In addition, the structural implications of such kinetic studies are, in many instances, correlated with molecular dynamics simulations (MD) and resonance Raman (RR) analyses (*26*, *27*).

Herein, we have extended our investigations of H_2S binding, stability, and release to and from hemeproteins by evaluating the effect of heme pocket mutations on the HbI−H_2S interaction using kinetics, MD simulations, and RR approaches. The results presented here show that (a) H_2S association is dictated by external kinetic barriers, (b) H_2S release is controlled by two competing reactions involving simple sulfide dissociation and heme reduction, (c) at high H_2S concentrations, reduction of the ferric center dominates, and (d) reduction of the heme is also enhanced in those HbI mutants having polar distal environments. On this basis, several factors controlling H_2S reactivity with hemeproteins were identified as follows: (i) accessibility of H_2S to the heme cavity, (ii) H_2S concentration, which stimulates electron transfer, (iii) the polarity of the distal environment surrounding the bound H_2S, and (iv) the stereo orientation of the distal side residues.

MATERIALS AND METHODS

Sample Preparation. Recombinant (rHbI) and mutant HbI constructs were prepared, expressed, and purified as described

previously (*28*). Briefly, HbI mutants were obtained by introducing single-amino acid substitutions into the HbI coding region that was obtained by RT-PCR amplification and cloned into the pET28(a+) vector using the Quick Change Mutagenesis kit (Stratagene, La Jolla, CA). The HbI mutants and rHbI were expressed in *Escherichia coli* Bli5 cells transformed with the constructs described above. Expression of the samples after induction with 1 mM IPTG yielded dark red cell pellets that were lysed and centrifuged to separate the soluble protein from the insoluble cell fractions as described previously (*28*). The soluble protein fractions were used for purification of the recombinant HbI proteins in Co^{2+} affinity columns (Talon, Invitrogen, Carlsbad, CA). Further purification of the samples was achieved by fast performance liquid chromatography (FPLC) in a Hi Load 26/60 Superdex 200 gel filtration column.

The carbon monoxide and oxygen derivatives were prepared by adding a slight excess of sodium dithionite (~50-fold) to the protein samples under anaerobic conditions followed by exposure to a CO or O_2 atmosphere. The identity of the CO and O_2 complexes was verified by their characteristic UV−vis spectra with distinct Soret bands at 420 and 416 nm, respectively (*16*). Carbon monoxide isotopic derivatives were formed in the same manner using $^{13}C^{18}O$ (Isotec). To form the metaquo complexes, a 10% excess of potassium ferricyanide was added to the protein samples. The HbI−H_2S derivatives were obtained by titrating small amounts of a 10 mM sodium sulfide solution with a gastight syringe into the deoxygenated metaquo−HbI samples (1−2 mM), until complex formation was attained. Typically, a 3−10-fold molar excess of H_2S was needed to form the complexes. The sodium sulfide solution was prepared by adding the salt, previously purged with N_2, to degassed and deoxygenated buffer to prevent oxygen contamination. The H_2S concentration of the sulfide solution was determined using the Apollo 4000 free radical analyzer. The UV−vis spectra of the samples were used to monitor formation of the H_2S derivatives, which show Soret and Q bands at 426 and 544 nm, respectively. The optical spectra of HbI−CO, HbI−O_2, metaquo, and HbI−H_2S derivatives were recorded using Shimadzu UV-2101PC and Agilent 8453 spectrophotometers.

Kinetic Measurements. The CO and O_2 association reactions were assessed with a flash photolysis system (Quantel) by photodissociating the HbI−CO or HbI−O_2 sample derivatives using 10 ns YAG laser pulses that provided 160 mJ at 532 nm. A low-intensity light source (50 W quartz halogen lamp filtered at 436 nm) was used as the probe beam, for samples in 1 mm cuvettes. All measurements were taken at 25 °C, in 50 mM phosphate buffer (pH 7.4). Kinetic curves were averaged with at least three traces recorded on a LeCroy 9400 oscilloscope. Oxygen dissociation rates (k_{off}) for all the HbI samples were measured by CO replacement techniques, as previously described (*29*). Samples with a slight excess of O_2 were mixed with buffer containing a high concentration of the competing ligand. Alternately, the oxygen k_{off} could be obtained from the observed replacement kinetics using the flash photolysis technique for samples under a mixed O_2/CO atmosphere. Analysis of the kinetics for the O_2 dissociation rates was conducted using simulations of double-exponential reactions to determine the kinetic constants.

The H_2S association rate constants (k_{on}) were obtained by measuring the reactions of the metaquo−HbI samples with H_2S solutions under anaerobic conditions, using a stopped-flow rapid scanning monochromator spectrophotometer (Olis-Online Instrument Systems, Bogart, GA) (*30*). The reactions were followed under pseudo-first-order conditions ($[H_2S] \gg [HbI]$) in which deoxygenated solutions of the metaquo−HbI samples at pH 6 were mixed rapidly with degassed solutions of sodium sulfide at different concentrations ranging from 0 to 4 mM. Data for the binding reactions were collected at 426 nm, the maximum in the static absorption of the HbI−H_2S spectrum, at a rate of 1000 scans/s. Dissociation of H_2S from the rHbI protein was first evaluated under equilibrium conditions. Initially, an ~3 μM deoxygenated and degassed metaquo−rHbI sample (1 mL) was mixed with a small amount of a 10 mM sulfide stock solution to yield a final H_2S concentration of 10 μM, which is the minimum H_2S concentration required to form the HbI−H_2S complex (3-fold molar excess). The sample was equilibrated, and then the absorption spectra associated with H_2S dissociation were recorded as a function of time for 5 h. The procedure was repeated using sulfide solutions with concentrations ranging from 20 μM (6-fold molar excess) to 5 mM (~2000-fold H_2S molar excess) to prepare the HbI−H_2S derivative. Hydrogen sulfide dissociation kinetics were then determined for rHbI and all the HbI mutants under anaerobic and aerobic conditions by monitoring the decay of the HbI−H_2S absorption signal for all the protein samples at 426 nm, using a UV−vis spectrophotometer (Agilent 8453). For the anaerobic measurements, small volumes (5 μL) of HbI−H_2S solutions (0.8−1.2 mM) were mixed rapidly with a large volume of deoxygenated buffer (1 mL) at pH 6.5 and the kinetic traces as well as spectra associated with the kinetics acquired for a period of 24 h. The H_2S dissociation kinetics under aerobic conditions were measured by mixing the HbI−H_2S samples with buffer saturated with O_2 instead.

Molecular Dynamics Simulations. Molecular dynamics simulations were performed for unligated ferric HbI and five point mutations at positions B10 and E11: PheB10Leu, PheB10Tyr, PheB10Val, PheE11Tyr, and PHeE11Val. These were carried out with AMBER version 7.0 (*31*). Initial coordinates for HbI were taken from X-ray structures (Protein Data Bank entry 1b0b). All mutants were generated with SCWRL version 3.0 (*32*). In all the MD calculations, the all-hydrogen topology with AMBER 94 (*33*) force field parameters and the TIP3P water model (*34*) were employed. Parameters around the iron and the charge set for heme in its Fe^{III} state were the same as in an earlier study of sulfide-binding hemoglobins (*35*). Each protein was solvated with explicit water molecules in a rectangular periodic box large enough to contain the protein and 10 Å of solvent on all sides. A 1400-step steepest-descent minimization was followed by a 1400-step conjugate gradient minimization, and the systems were then heated for 50 ps to a final temperature of 300 K. During the heating, a harmonic constraint of 200 kcal $Å^{-2}$ mol^{-1} was applied to the protein atoms. For all the mutants, the residue at the point mutation position was not constrained. The time step was 2 fs, and the SHAKE algorithm was employed to constrain bonds involving hydrogen atoms. A cutoff of 10 Å was applied to nonbonded interactions. All the systems were equilibrated for 500 ps before each 1 ns trajectory was started. Data were collected at 1.0 ps intervals. During the simulations, the temperature was held constant al 300 K by the weak coupling algorithm (*36*) with a time constant for heat bath coupling (τ) of 2.0 ps.

Resonance Raman Measurements. The RR spectra of the CO−, metaquo−, and H_2S−rHbI and −HbI mutant proteins (heme concentration of ~100 μM) were obtained using a 413.1 nm excitation line from a Kr^+ ion laser with a power of

10 mW (Spectra Physics). The laser was focused to an ~30 μm spot on the rotating cell to prevent photodamaging. A back-illuminated CCD detector (800 × 2000 pixels), coupled to a modified Spex 1401 and notch filters centered at 410 nm, was used to record the RR spectra. For the CO and metaquo samples, three spectra were collected and averaged, each composed of 60 accumulations of 10 s. On the other hand, 30 single spectra consisting of six accumulations at 10 s each were obtained for the HbI−H_2S derivatives. The Raman shift was calibrated using indene for both the low- and high-frequency regions.

RESULTS

Functional and Structural Features of the Ferrous Derivatives. To define the reactivity of H_2S with HbI as well as the HbI mutated systems, and to extrapolate the results to other hemeproteins, it is necessary to have an initial perspective on how the structure and electronic environment of these pockets behave in the presence of common ligands such as CO and O_2. Thus, the kinetics and structural analyses of each HbI mutant as well as rHbI were first evaluated with CO and O_2. The microsecond bimolecular time courses for binding of CO and O_2 to rHbI and HbI mutants followed simple pseudo-first-order kinetics, and the traces were therefore fitted with single-exponential functions. Figure 2 shows the comparison of CO binding for rHbI and several HbI mutants. Substitution of GlnE7 with a smaller residue such as Val or Asn increases the k_{on} by a factor of 20 or 4, respectively. An opposite effect is observed for the bulkier and polar GlnE7His mutant, in which a 15-fold decrease in the CO association constant is observed. The results demonstrate a direct correlation between the size of the E7 residue and CO binding to the heme center. For the B10 mutations, single Phe substitution with the polar aromatic acid, Tyr, decreased the CO association constant from 7.2×10^6 to 6.5×10^5 M^{-1} s^{-1}. This result can be explained by fact that in this mutant, the tyrosine residue is in the proximity of the heme iron (*19*), thus obstructing CO entry. Mutation of PheB10 to Val or Leu, however, did not affect the CO association constant significantly despite their differences in size and volume (23.2 Å for the Phe to Leu mutant and 49.9 Å for the Phe to Val mutant) (*37*). This suggests that CO entry is not directly modulated by the size of the B10 residue. Intriguingly, replacing PheE11 with either Val or Tyr, each of which differs from the other in size and polarity, provoked similar increases in the CO binding constants ($16-17 \times 10^6$ M^{-1} s^{-1}). Consequently, this indicates that these mutations may induce analogous structural rearrangements within the distal pocket that indirectly modulate CO entry with respect to rHbI, as judged by the 2-fold increase in the k_{on} value. For SWMb, mutation of either LeuB10 or ValE11 with Phe reduces the CO k_{on} by a factor of 2, implying that the binding of the ligand is sensitive to the size of the residues occupying those positions (*24*). The observation that replacement of PheB10 and PheE11 in HbI does not affect directly CO association while a direct correlation is observed for SWMb accentuates the different local structure of their heme pockets.

Oxygen association kinetics of rHbI and various site-directed mutants are shown in Figure 2B. The O_2 k_{on} values of the E7 variants follow the trend observed for CO binding in which an increase in the k_{on} is observed for the GlnE7Val and GlnE7Asn mutants while a 6-fold decrease in this value is observed for GlnE7His. Similar to that of CO, a substantial decrease in the O_2 k_{on}, from 1.9×10^8 to 6.8×10^6 M^{-1} s^{-1}, is also observed for the

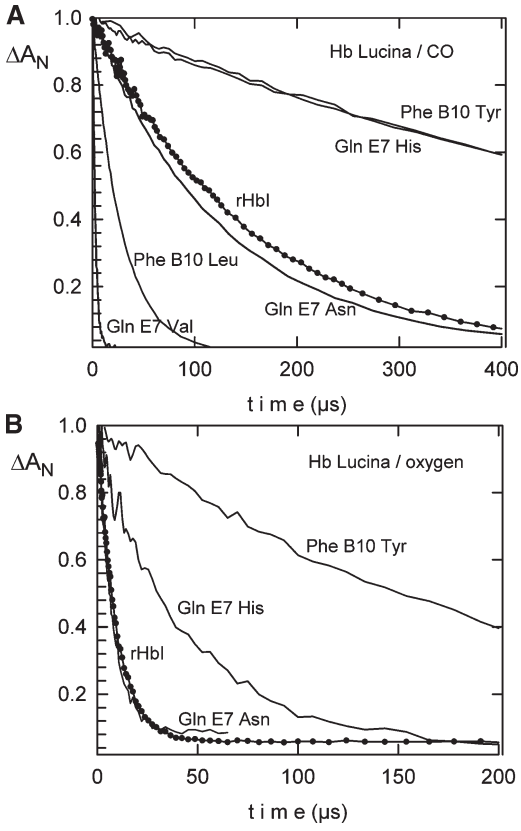

FIGURE 2: (A) Bimolecular kinetics for rebinding of CO to rHbI and several Hb site-directed mutants. Samples of 10 μM hemeprotein were monitored at 436 nm. The conditions for all reactions were 50 mM sodium phosphate at pH 7.4 and 25 °C under air or 1 atm (1000 μM) of CO. (B) Bimolecular kinetics for O_2 recombination after photolysis of rHbI and the distal GlnE7His, PheB10Tyr, and PheE7Asn mutants, for samples under air.

PheB10Tyr mutant. Substitutions of PheB10 with Val or Leu and PheE11 with Val or Tyr caused only minor changes in O_2 association rate constants. For instance, a slight increase in O_2 k_{on} from 1.9×10^8 to 2.3×10^8 M^{-1} s^{-1} is observed for the PheB10Leu mutant, while similar constants are obtained for the PheB10Val, PheE11Val, and PheE11Tyr variants (near 1.1×10^8 M^{-1} s^{-1}). Since the association kinetics of both ligands are affected in a similar fashion, a simple steric model seems appropriate in which higher rates are observed for smaller residues at position E7: GlnE7Val > GlnE7Asn > rHbI > GlnE7His. Accordingly, these results suggest that binding of CO and O_2 to the ferrous HbI mutants is controlled mainly by steric constraints rather than electronic, in which GlnE7His reduces the free available space in the HbI distal pocket delaying, in turn, ligand binding. Mutating PheB10 to Tyr also diminishes the ligand association due to steric hindrance. In contrast, the CO and O_2 association constants for the PheB10Leu, PheB10Val, and E11 mutations do not systematically depend on the size or polarity of the residues occupying those positions. This implies that these B10 and E11 substitutions may stimulate structural displacements that can in turn affect CO and/or O_2 binding relative to rHbI.

Table 1 summarizes the oxygen dissociation rate constants for rHbI and several HbI mutants (*23*). In this regard, it has been shown that the dissociation of O_2 from the HbI mutants depends strongly on the hydrogen bonding interaction between the E7 residue and the bound ligand (*21*, *23*). In brief, the 72 and 63% increases in the O_2 k_{off} observed for the GlnE7Val and GlE7Asn

Table 1: CO, O_2, and H_2S Association Rate Constants of the rHbI and HbI Mutants (O_2 dissociation also shown)

protein	CO k_{on} ($\times 10^6$ M^{-1} s^{-1})	O_2 k_{on} ($\times 10^6$ M^{-1} s^{-1})	O_2 k_{off} (s^{-1})	H_2S k_{on} ($\times 10^3$ M^{-1} s^{-1})
wtHbI[a]	0.5	100−200	61	27.30[c]
rHbI	7.2	190	140[b]	24.30[c]
ValE7	160	490	500[b]	276.78
AsnE7	31	230	375[b]	39.15
HisE7	0.47	31	3[b]	65.80
LeuB10	7.4	230	300[b]	61.75
ValB10	9.0	110	400	nd[d]
TyrB10	0.65	6.8	0.6[b]	3.94
ValE11	16	120	325	16.95
TyrE11	17	110	40	11.46

[a] Data from ref *16*. [b] Data from ref *23*. [c] Data from ref *30*. [d] Not determined.

mutants were attributed to a complete or partial removal of the hydrogen bond between the bound ligand and these residues, respectively, while the decrease of this value by a factor of 47 in the GlnE7His variant was ascribed to a strong hydrogen bond (*21*). A strong H-bond between the bound O_2 and the PheB10Tyr mutant was also suggested in this study, which decreased the dissociation rate by a factor of 233. Both the His and Tyr residues of the GlnE7His and PheB10Tyr mutants were implicated in a strong O_2 stabilization mechanism, while a moderate stabilization role was attributed to GlnE7 in rHbI (*21*). The results collected here show that that replacing PheB10 and PheE11 with a smaller and nonpolar residue such as Val induces a 57−65% increase of the O_2 dissociation rate (from 140 to 325−400 s^{-1}). The faster O_2 dissociation behavior observed in these mutants can be rationalized in principle by the loss of multipole interactions generated by the Phe cage (*22*, *23*). However, the energy associated with these aromatic−electrostatic interactions (~1.5 kcal/mol) (*18*) appears to be insufficient to provoke these 57−65% increases in the rate of O_2 release, which are similar to that obtained for the partial removal of the H-bond in the GlnE7Asn mutant (63%). Thus, the data suggest that a weakening of the hydrogen bonding interaction between GlnE7 and O_2 may also occur in these mutants due to the movement of the GlnE7 amide group away from the binding site. This displacement, induced by the PheB10 and PheE11 substitutions, supports the idea that distal structural rearrangements occur in these mutations. Consequently, these results indicate that both factors affect O_2 dissociation, which is consistent with previous reports (*23*, *38*) in that GlnE7 is responsible for modulating O_2 stabilization in HbI and PheB10 and PheE11 are also involved in this process. The apparent role of PheB10 and PheE11 in O_2 stabilization has also been suggested before in a SWMb triple mutant that mimics the HbI active center (HisE7Gln, LeuB10Phe, and ValB10Phe) (*39*). In this Mb mutant, a 4-fold decrease in O_2 k_{off} was observed when compared to that of wtSWMb, indicating that PheB10 and PheE11 are responsible for ligand stabilization and release in this variant. The distal structural changes suggested in the CO and O_2 kinetic analyses described above for the PheB10Leu, PheB10Val, and E11 mutants and the stabilization roles of residues E7, B10, and E11 proposed in the dissociation studies may be important factors in determining the extent of interactions of H_2S with hemeproteins. Therefore, to corroborate these kinetic interpretations, the structural properties of the rHbI−CO and HbI−CO mutated systems were examined by measuring their RR scattering responses.

Figure 3 shows the RR spectra of the CO-bound rHbI and mutant derivatives. The low-frequency spectrum of rHbI (top trace in Figure 3A) demonstrates a band at 516 cm^{-1}, which was formerly attributed to the Fe−C stretching mode (ν_{Fe-C}) of the wtHbI−CO complex (*38*). Panel B in Figure 3 shows that this band shifts to a lower frequency upon isotope substitution ($^{12}C^{16}O$ vs $^{13}C^{18}O$), thus confirming the previous assignment. At higher frequencies, the spectrum of rHbI shows an additional isotope sensitive band at 1945 cm^{-1} as demonstrated in the top trace of Figure 3C and is assigned here to the C≡O stretching mode ($\nu_{C\equiv O}$). Both ν_{Fe-C} and $\nu_{C\equiv O}$ in the low- and high-frequency regions, respectively, are significantly affected with distal site mutations as indicted in Figure 3. Replacing GlnE7 with Val induces a shift of the ν_{Fe-C} low-frequency mode to 504 cm^{-1} as well as a displacement of the $\nu_{C\equiv O}$ high-frequency mode to 1962 cm^{-1}. Mutating GlnE7 to Asn also provokes a shift of ν_{Fe-C} to 507 cm^{-1}, while the $\nu_{C\equiv O}$ mode is observed in the high-frequency region of the spectrum at 1946 cm^{-1}. In contrast, Figure 3 shows that the GlnE7His variant shows two isotope sensitive lines for ν_{Fe-C} and $\nu_{C\equiv O}$ modes at 502 and 1965 cm^{-1} and at 530 and 1930 cm^{-1}, respectively, with the latter pair dominating the isotope difference spectra. The data thus far show that replacing GlnE7 with nonpolar residues decreases the ν_{Fe-C} and increases the $\nu_{C\equiv O}$ mode, respectively, while the opposite effect is observed for more polar substitutions.

This trend is analogous to that observed in many hemeproteins (Figure 4), including Mb mutants (*26*), in which replacement of HisE7 with nonpolar residues shifts the ν_{Fe-C} (512 cm^{-1}) to lower frequencies while displacing the $\nu_{C\equiv O}$ (1944 cm^{-1}) to higher values (*27*). Furthermore, substitution of HisE7 in Mb with more polar residues had the opposite effect. This phenomenon has been very well established, and it indicates loss or gain of H-bonding interactions that could stabilize the bound CO. Hence, the displacements of the ν_{Fe-C} and $\nu_{C\equiv O}$ modes observed in the GlnE7Val and GlnE7Asn variants to lower and higher frequencies, respectively, imply loss or weakening of H-bonding interaction between the E7 residue and the CO ligand, confirming the role of GlnE7 in the stabilization of ligands (Figure 4). On the other hand, the shift of these modes to higher and lower frequencies in GlnE7His indicates a stronger ligand stabilization mechanism in comparison with that of rHbI. The HbI PheB10 mutants exhibit a similar tendency. For instance, substitution of PheB10 with nonpolar Leu or Val in HbI produced the same spectral changes, showing the ν_{Fe-C} mode at 504 cm^{-1} and the $\nu_{C\equiv O}$ mode at ~1944 or 1946 cm^{-1}, respectively, implying loss of a positive distal site environment. The data also confirm the importance of PheB10 in stabilizing the bound ligand through the aromatic multipole interactions. Moreover, the substantial shift of the ν_{Fe-C} mode (504 cm^{-1} for the mutants and 516 cm^{-1} for rHbI) and the identical spectral features of the PheB10Leu and PheB10Val variants support the notion that these mutations provoke analogous conformational changes, involving movement of the GlnE7 amide group, that weaken further the H-bonding interaction with the bound ligand. On the other hand, the polar PheB10Tyr mutant produced shifts in the ν_{Fe-C} and $\nu_{C\equiv O}$ modes to 541 and 1925 cm^{-1}, for the low- and high-frequency regions, respectively, indicating a strong positive field in the vicinity of the ligated CO.

Interestingly, this trend of an increasing ν_{Fe-C} with a decreasing $\nu_{C\equiv O}$ upon polar residue replacement is not observed in the

HbI PheE11 variants. As Figures 3 and 4 show, substitution of PheE11 with a nonpolar Val or polar Tyr residue yields similar low-frequency ν_{Fe-C} modes at 514 cm^{-1} and high-frequency $\nu_{C\equiv O}$ modes at 1944 and 1940 cm^{-1}, implying that these modes are less sensitive to the polarity of the residues occupying this position. Nonetheless, as in the PheB10Val and PheB10Leu mutants, the similarities in spectral behavior of these E11 variants and the small shift of both modes when compared to rHbI (514 cm^{-1} vs 516 cm^{-1}) suggest related structural changes that induce a slight loss of the positive field surrounding bound CO. Taken together, these RR results support the idea drawn from the kinetic analyses in that (i) GlnE7His and PheB10Tyr exert stronger stabilization mechanisms with bound ligands, (ii) a distal structural rearrangement, involving GlnE7, occurs in the PheB10Leu, PheB10Val, and E11 mutations, and (iii) GlnE7, PheB10, and PheE11 contribute synergistically to the stabilization of the ligand in deoxyHbI. These results along with those obtained in the association kinetic study provide the structural information associated with the HbI mutants that can in turn affect the interaction of HbI and its site-directed mutants with H_2S in a ferric heme pocket environment.

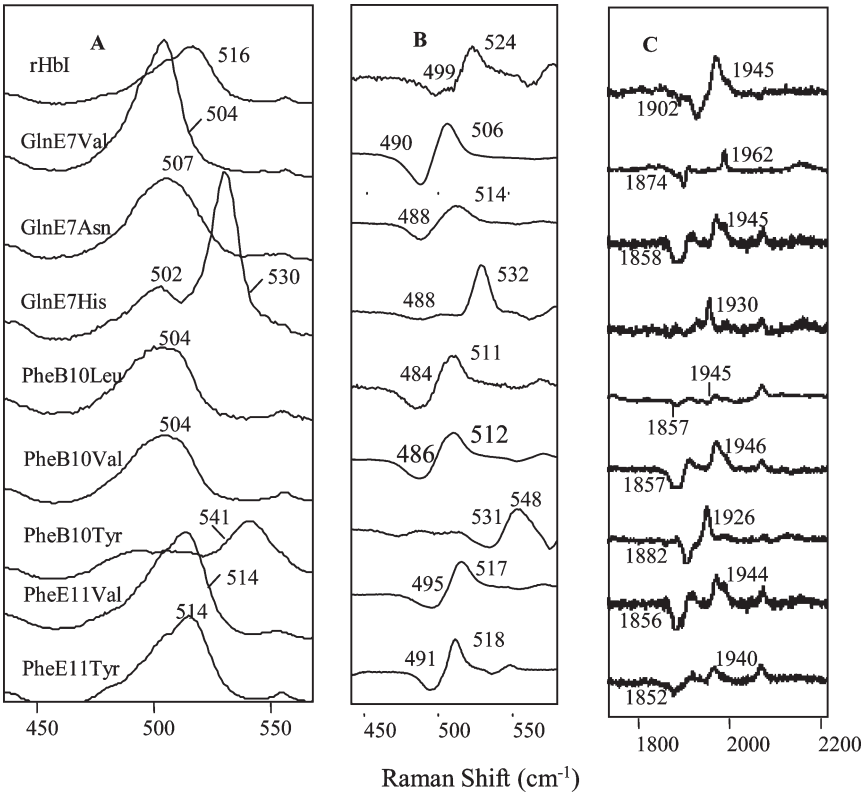

FIGURE 3: Resonance Raman spectra of the HbI−CO protein samples: (A) low-frequency region and (B and C) $^{12}C^{16}O - {}^{13}C^{18}O$ isotope difference spectra of the low- and high-frequency regions, respectively. Some of the spectra in panel C show flat peaks due to the subtraction process.

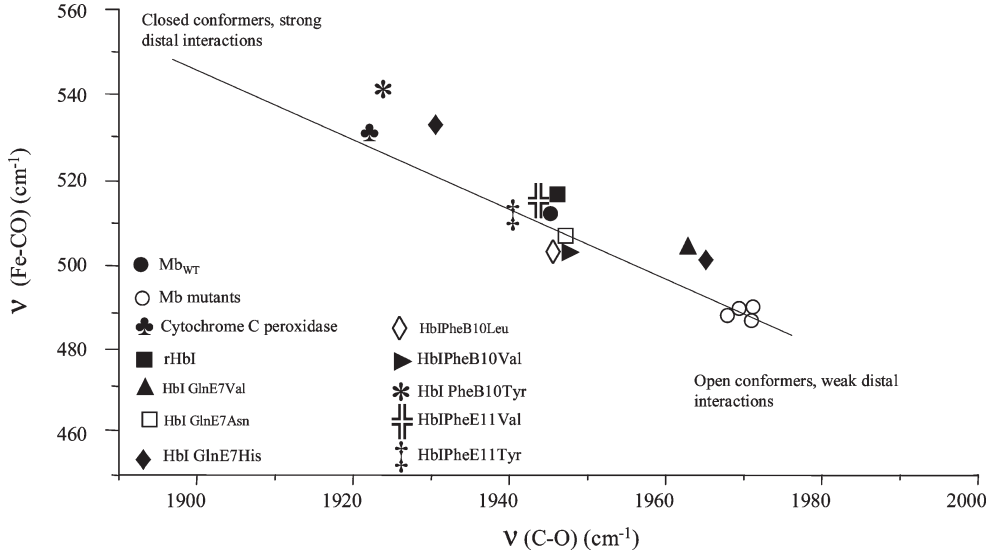

FIGURE 4: ν_{Fe-C} vs $\nu_{C\equiv O}$ inverse correlation curve for Mb, Mb mutants, cytochrome *c* peroxidase, and the HbI proteins.

Structural Aspects of the Metaquo Derivatives. The direct steric constraint suggested in the CO and O_2 association kinetics for the GlnE7His and PheB10Tyr mutants, relative to rHbI, and the strong stabilization mechanisms invoked for these variants in the ferrous dissociation and RR studies are important factors that can affect the nature of H_2S binding and release in HbI and consequently in hemeproteins. Moreover, the distal conformational changes inferred from the ferrous kinetic and RR analyses upon B10 and E11 substitutions not only can alter H_2S interaction but also can help to define the different responses exerted by this ligand in hemeproteins. Hence, to identify the structural properties of the HbI mutants in the ferric environment and to estimate how they will influence H_2S stability and release, the resonance Raman scattering of several metaquo−HbI mutant derivatives was measured in the high-frequency region. The high-frequency region of the metaquo RR spectra provides information about the overall heme environment, and it was used here to characterize the ferric structural features of the HbI mutant complexes in comparison with the wtHbI previously reported (*38*).

Figure 5 shows the high-frequency RR spectra of the metaquo−GlnE7Val, −PheB10Tyr, −GlnE7His, and −PheB10Val HbI mutated systems. Similar to that of wtHbI (*38*), the oxidation state marker band, ν_4, for the mutated systems presented in Figure 5 appears at 1371 cm^{-1}, demonstrating the presence of heme−Fe^{III} derivatives. The RR scattering of rHbI, GlnE7Val, and PheB10Tyr shows that the ν_3 and ν_2 modes at 1480 and 1560 cm^{-1} dominate the spectra. A small contribution of the low-spin, six-coordinate metaquo species is also observed in these protein samples as indicated by the ν_2 mode at 1580 cm^{-1}. Such mixtures, involving the presence of a small population of the low-spin state, are typical of metaquo complexes with the water molecule occupying the six coordination position. The spectra of the PheB10Val and GlnE7His mutants also display the ν_3 and ν_2 modes at 1480 and 1560 cm^{-1}, respectively, indicative of high-spin, six-coordinate metaquo species as well. However, substantial increases in the magnitudes of the ν_3 and ν_2 markers at 1505 and 1580 cm^{-1}, respectively, are observed, suggesting a stronger contribution of the low-spin, six-coordinate metaquo species in these variants. These results suggest that in PheB10Val and GlnE7His, the water molecule is coordinated to the heme distal site with an equal mixture of high- and low-spin configurations. Resonance Raman studies of various metaquo−hemoglobin derivatives showing a strong contribution of the low-spin state, such as the truncated Hb from the protozoan *Paramecium caudatum* (trHbP) (*27*) and a HisE7Arg SWMb mutant (*40*), have indicated that the low-spin character of the mixture arises from H-bonds between heme-bound water and the distal residues. These H-bonding interactions increase the ligand field strength, increasing in turn the level of the low-spin state of the complexes. Therefore, the strong contribution of the low-spin markers in the GlnE7His variant can then be rationalized by the formation of a strong hydrogen bond between the imidazole side chain and the water-bound molecule, which generates a strong ligand field and increases the low-spin character of this derivative. In the PheB10Val mutant, the best explanation for the strong low-spin contribution is that movement of GlnE7 toward the ferric iron may induce the generation of a strong H-bond between this residue and H_2O that stabilizes the low-spin state of this complex. Similar H-bonding interaction can be predicted in these Hb−H_2S mutant derivatives, which may alter in turn sulfide stabilization and release. In addition, these results demonstrate

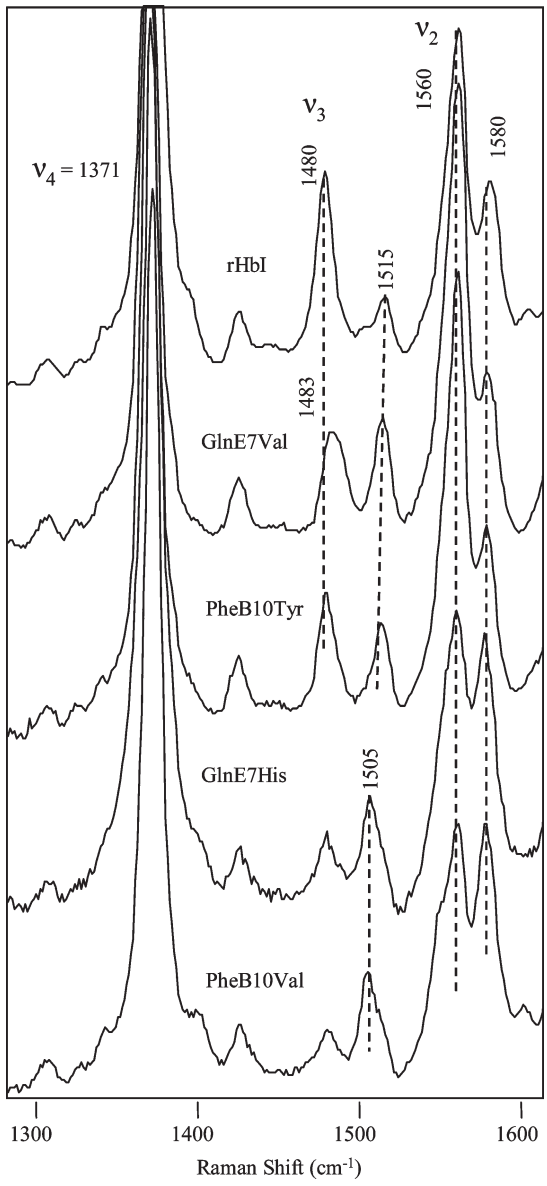

FIGURE 5: High-frequency resonance Raman spectra of the metaquo derivatives for some of the HbI mutants, showing the ν_3 and ν_2 modes.

that, in agreement with the ferrous analyses, the PheB10Val mutation stimulates structural changes within the heme distal site that can affect ligand dissociation. These alterations are also expected to occur in PheB10Leu and the E11 mutants. To assert this hypothesis, molecular dynamics simulations of these ferric HbI mutants were conducted.

The MD results demonstrate that in the PheB10 and PheE11 mutations a structural rearrangement of GlnE7 occurs. As panels C and D of Figure 6 show, in wtHbI the GlnE7 dihedral angle χ_1 is found to be 180°, while a 90° rotation about this angle is predicted for the PheB10 and PheE11 mutants. The consequence of this rotation would be a reorientation of the GlnE7 C═O side chain. For instance, panels A and B of Figure 6 show that the distribution of the GlnE7 carbonyl group angle with respect to the ferric iron center varies substantially in these B10 and E11 mutants. The C═O(GlnE7)−Fe angle changes from ~90° to 180° in the PheB10Val and PheB10Leu mutants with the C═O pointing toward the ferric iron. Although less dramatic, similar changes are observed for the PheE11Val and PheE11Tyr variants. This is in good agreement with the previous suggestion, in

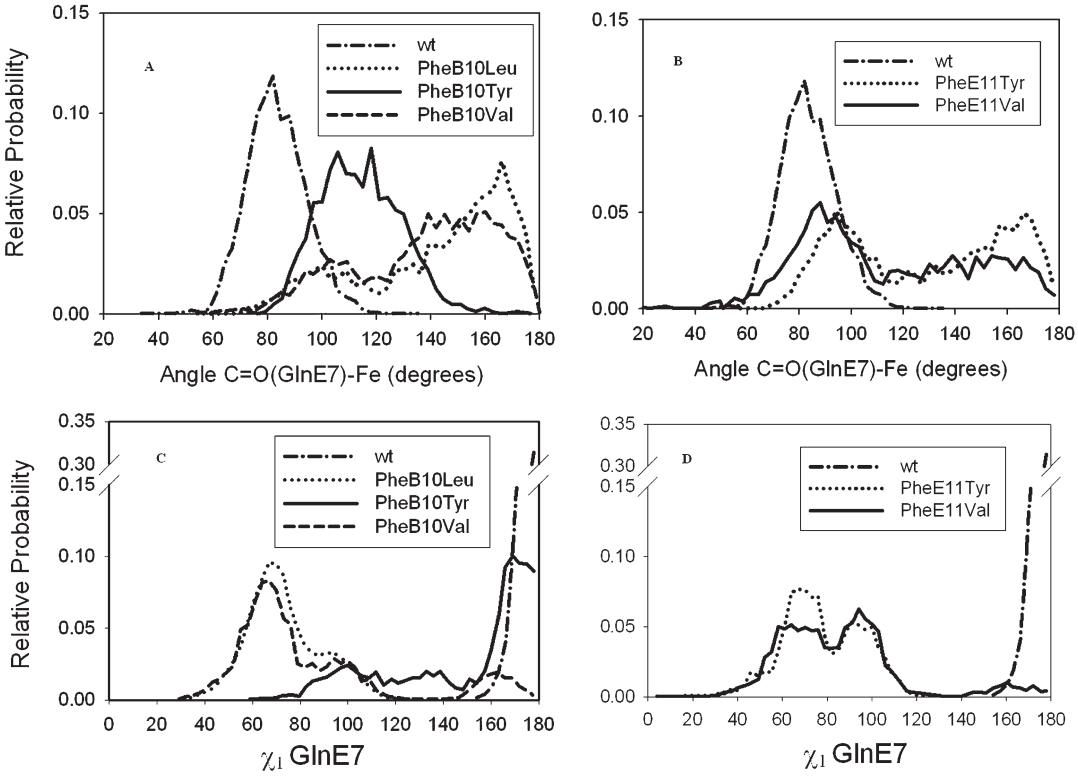

FIGURE 6: Histograms for GlnE7 dihedral angle χ_1 and the angle associated with the carbonyl group of GlnE7 and the heme iron. Panels A and B display the C═O(GlnE7)−Fe angles for the B10 and E11 mutants, respectively, while panels C and D show the χ_1 GlnE7 dihedral angles of the same variants.

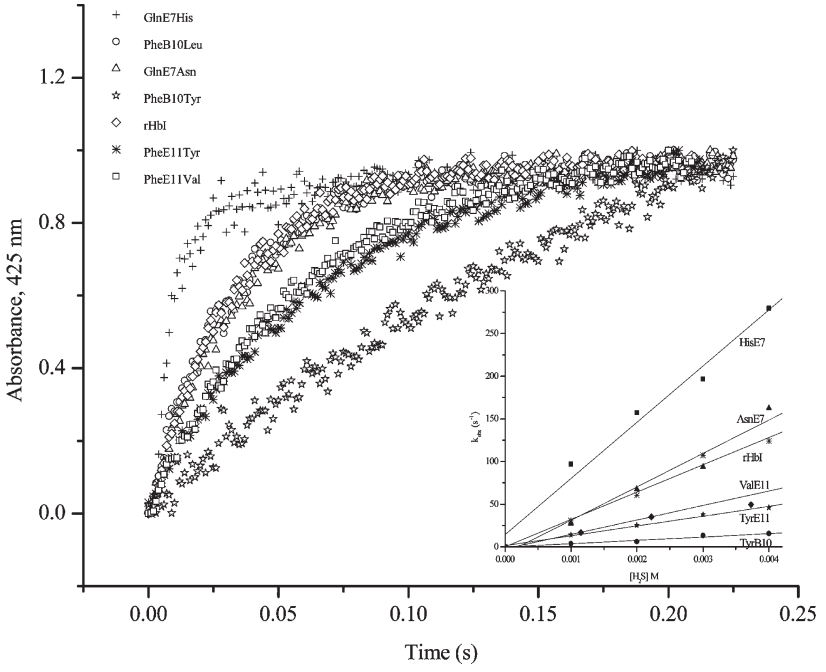

FIGURE 7: Hydrogen sulfide association kinetics of rHbI and the mutated samples. The inset displays the plot of the observed rate constants as a function of H_2S concentration.

which these B10 and E11 mutants alter the HbI distal structural environment affecting ligand entry and release from the heme pocket. Furthermore, the data also set the stage for defining how these perturbations induced by the mutations can affect the interaction of H_2S with the ferric heme center.

Interaction of H_2S with the Metaquo Derivatives. The RR results of the metaquo−HbI mutants presented above suggest that the reactivity of H_2S may be modulated in the GlnE7His and PheB10Val mutants relative to the rHbI, due to their differences in the distribution of the high- and low-spin configurations. The data along with the MD simulations also indicate that PheB10Val, PheB10Leu, and E11 mutations produce distal conformational changes that can modify H_2S binding and stability as well. To identify how these findings influence H_2S

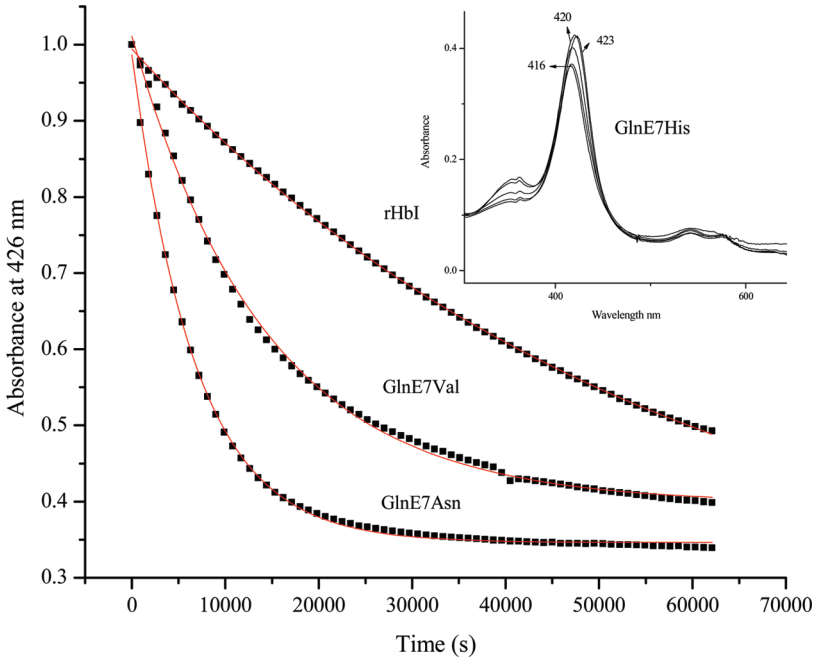

FIGURE 8: Dissociation kinetic traces of rHbI, GlnE7Asn, and GlnE7Val. The inset shows the spectra related to kinetics of dissociation of H_2S for the GlnE7His mutant under aerobic conditions.

reactivity with metaquo−rHbI and the HbI site-directed mutants, sulfide dissociation kinetics as well as RR measurements were conducted. In addition, the effects of these mutations on H_2S binding were evaluated.

Figure 7 shows the comparison of the H_2S association kinetics of the metaquo−rHbI derivative previously reported (*30*) and various HbI mutants studied here. All the traces followed a single kinetic event, indicating that the ligand reacts readily with the ferric heme center. The calculated association rate constants for each protein were obtained by fitting the data with single-exponential functions and plotting the observed constants, k_{obs}, as a function of H_2S concentration as shown in the inset. The binding constants thus obtained are summarized in Table 1. Evaluation of the association constants for the E7 mutants demonstrates that replacing GlnE7 with Val, Asn, or His increases the association constant by a factor of 11, 2, or 2.7, respectively. As opposed to CO and O_2 binding, there is not a direct correlation between the size of the E7 residue and H_2S binding to the heme center, suggesting that its association may also be governed by an external kinetic barrier. In this respect, transient fluctuations of the protein may be as important as steric effects for H_2S binding, probably because of the larger nature of the ligand itself. The results show that H_2S binding is nearly 1000 times slower that CO and O_2, suggesting that protein fluctuations are required to allow H_2S access to the iron−heme center. That could explain why the GlnE7His mutant seems too fast for H_2S while it is the slowest E7 mutant for CO and O_2 binding.

Mutation of PheB10 to Leu increases the association constant from 2.43×10^4 to 6.58×10^4 M^{-1} s^{-1}, while substitution of this residue with Tyr decreases the k_{on} value by a factor of 6. This suggests that once H_2S is inside the protein, its binding may be dictated by the free accessible space in the distal site.

Interestingly, substitution of PheE11 with a much smaller nonpolar residue such as Val instead of increasing the H_2S association constant, as observed in the GlnE7Val mutant, decreases this value from 2.43×10^4 to 1.69×10^4 M^{-1} s^{-1}. Similarly, the association rate of the PheE11Tyr mutant decreases 2-fold to 1.15×10^4 M^{-1} s^{-1}. Hence, like deoxy CO and O_2, the structural displacements caused by these E11 mutations affect entry of the ligand into the heme distal site. Overall, our results show that H_2S association is influenced by an outer kinetic barrier that requires transient motions of the protein to allow its movement into the distal pocket. Once H_2S is inside the protein, its binding is controlled by either electronic or steric constraints exerted by nearby residues.

Dissociation of H_2S from rHbI was studied first under equilibrium conditions using the lowest sulfide concentration required to form the complex (10 μM or a 3-fold H_2S molar excess). Under these conditions, dissociation of H_2S from rHbI showed a tendency toward formation of a metaquo complex, as judged by the 425 to 408 nm displacement of the Soret band. However, a broad Soret band was observed, suggesting that other processes may be contributing to H_2S dissociation. Similar results were observed using H_2S concentrations ranging from 20 to 480 μM, corresponding to 6- to 160-fold sulfide molar excesses, respectively, to form the complex. At higher sulfide concentrations (600 μM to 5 mM, equivalent to 200−2000-fold H_2S molar excesses, respectively), dissociation of H_2S from rHbI, at equilibrium, revealed the formation of a final deoxy-like species with Soret and Q bands at 433 and 560 nm, respectively, indicating reduction of the heme−iron center (figure not shown). Hence, the data suggest that H_2S dissociation under equilibrium conditions is dominated by two competing reactions involving simple release of H_2S from the ferric iron and reduction of the heme iron followed by H_2S liberation. At low H_2S concentrations, the former process seems to dictate the dissociation reaction, while the latter reduction process appears to dominate at higher sulfide concentrations. The H_2S dissociation kinetics of the rHbI and the HbI mutants were therefore measured at the limit of complex formation (3−10-fold molar excess) to minimize the difficulties associated with competing reactions such as heme reduction.

Figure 8 shows the dissociation kinetic traces for rHbI, GlnE7Asn, and GlnE7Val. The calculated dissociation constants, obtained by fitting the traces with single-exponential

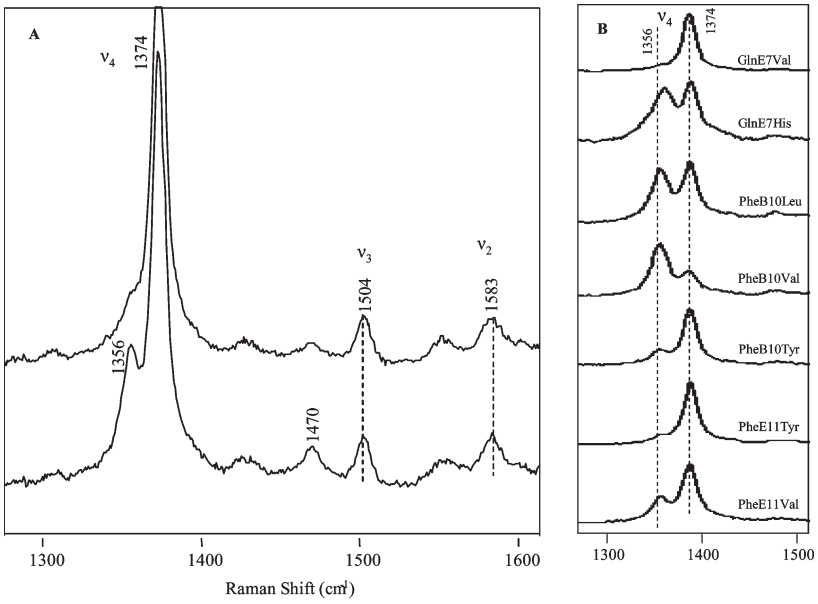

FIGURE 9: High-frequency resonance Raman spectra of the rHbI−H_2S and mutant derivatives. The top trace in panel A is the first spectrum recorded upon reaction of H_2S with the sample, while the second one is the last spectrum taken (after 30 min). The ν_4, ν_3, and ν_2 modes are highlighted. Panel B shows the high-frequency resonance Raman spectra of various HbI−H_2S mutants, showing the contribution of the ν_4 band at 1356 cm^{-1}, characteristic of deoxy species.

functions, are 0.03×10^{-3}, 0.15×10^{-3}, and 0.06×10^{-3} s^{-1} for rHbI, GlnE7Asn, and GlnE7Val, respectively. The results show an increase in H_2S k_{off} of 80% in GlnE7Asn probably due to a substantial weakening of the strength of the hydrogen bond between this residue and the bound ligand. An increase in k_{off} is also observed for the GlnE7Val mutant, but it is not as significant as that for the Asn mutant (80% vs 50%), suggesting that the other competing reaction (heme reduction) is also contributing to the observed signals. In fact, the spectra associated with these kinetics showed a final broad Soret band centered at 409 nm supporting the suggestion made above. Furthermore, the kinetic spectra of the GlnE7His mutant under aerobic conditions showed that an intermediate is formed rapidly and decays to form a new species with a characteristic Soret band at 416 nm (inset in Figure 8). Additionally, the kinetic trace of dissociation of H_2S from GlnE7His shows much more complex behavior and could not be fitted with a single exponential. Similar difficult kinetic traces are observed for the B10 and E11 mutated systems studied. These data were therefore fitted with a double-consecutive exponential function, yielding constants for the first and second phases. The constants thus obtained do not correlate with any physical or chemical properties of the mutated residues. However, the 416 nm Soret band in the GlnE7His mutant suggests that an oxy-like species may be formed, indicating that reduction of the heme−Fe^{III}−H_2S moiety dominates in this mutant even at the minimum H_2S concentration needed to form the complex (3−10-fold molar excess). We thus hypothesize that in rHbI and the HbI mutants both competing processes are involved in H_2S dissociation and that the contribution of heme reduction depends strongly on the distal site environment. To corroborate this interpretation, resonance Raman studies of these derivatives were performed. The sensitivity of RR spectroscopy for studying heme structural properties, as opposed to UV−vis, should yield relevant information associated with the H_2S dissociation kinetics described above.

The high-frequency RR spectra obtained upon reaction of H_2S with metaquo−rHbI is shown in Figure 9A. The top trace shows the oxidation state marker at 1374 cm^{-1}, characteristic of a Fe^{III}−heme protein. The presence of the ν_3 and ν_2 modes at 1504 and 1583 cm^{-1}, respectively, indicates a low-spin six-coordinate metsulfide HbI complex. Interestingly, the bottom trace shows that the HbI−H_2S complex changes within a few minutes, indicating the presence of a mixture of a deoxy high-spin species and a metsulfide derivative as evidenced by the appearance of new oxidation and spin markers at 1356 and 1470 cm^{-1}, respectively. Figure 9B demonstrates similar results for all the mutant proteins studied. Laser power dependence studies indicate that this reduction process is power-independent (data not shown), but it depends strongly on distal site mutations. The tendency toward $Fe^{III}H_2S$ reduction for all the site-directed mutants studied is as follows: PheB10Val > PheB10Leu ≈ GlnE7His > PheE11Val > PheB10Tyr > PheE11Tyr > rHbI > GlnE7Val. This reduction process is also confirmed by the instantaneous appearances of the ν_{Fe-His} frequency in the low region at 219 cm^{-1} (data not shown). The data confirm the dissociation kinetic analyses in that reduction of the heme iron takes place in HbI and the HbI mutated systems at the limit of H_2S concentrations for complex formation. Furthermore, the results show that HbI distal site mutations induce different structural conformations that affect the nature of H_2S reactivity as described in detail below.

DISCUSSION

Distinct Distal Structural Geometry Influences H_2S Reactivity in Hemeproteins. The kinetics and RR results obtained with the ferrous HbI mutant derivatives, which are summarized in Tables 1 and 2, respectively, show that mutating E7, B10, and E11 provokes different heme distal structures that influence directly or indirectly the extent of interaction of CO and O_2 with the ferrous iron center. The data reveal that relative to rHbI and GlnE7Val, His and Tyr in the ferrous GlnE7His and PheB10Tyr variants diminish the amount of free available space in the HbI distal pocket that reduce CO and O_2 binding. Upon CO and O_2 coordination, GlnE7His, PheB10Tyr, and wtHbI form H-bonding interactions with the bound ligands generating

closed distal cavity configurations. On the other hand, no CO and O_2 stabilization is invoked in GlnE7Val, inducing in turn an open distal structure. For the PheB10Val, PheB10Leu, and E11 variants, the data show that they do not directly dictate ligand binding and release; instead, these mutations induce distal structural rearrangement that affects indirectly both ligand entry and release.

Distinct structural geometries are also observed in the ferric HbI mutants. With regard to this, the equal contributions of spin states illustrated in the RR spectra of metaquo−GlnE7His and the PheB10Val mutant derivatives suggest that two individual distal structures coexist in a conformational equilibrium relative to the metaquo−wtHbI, GlnE7Val, and PheB10Tyr derivatives. One of these structures is associated with H-bonding interactions between the HisE7 and the bound water in the GlnE7His mutant and with GlnE7 and the coordinated ligand in the PheB10Val variant, with this latter interaction being induced by the Val replacement. As depicted in Figure 10, substitution of PheB10 with Val resulted in a stereo orientation of GlnE7 different from that of wtHbI, where the carbonyl group points toward the heme.

Table 2: Selected RR Band Assignments for the CO− and H_2S−HbI Mutant Derivatives

	CO		H_2S		
protein	ν_{Fe-CO}	ν_{c-o}	ν_2	ν_3	ν_4
wtHbI[a]	516	1945	1579	1500	1372
rHbI	516	1945	1583	1504, 1470	1374 (87%)[b]
					1356 (13%)
ValE7	504	1962	1580	1501	1372
AsnE7	507	1946	nd[c]	nd[c]	nd[c]
HisE7	502	1965	1583	1505, 1470	1373 (53%)
	532	1930			1356 (47%)
LeuB10	504	1944	1583	1502, 1470	1373 (53%)
					1355 (47%)
ValB10	504	1946	1582, 1562	1500, 1470	1372 (32%)
					1355 (68%)
TyrB10	541	1925	1583	1503. 1470	1372 (80%)
					1354 (20%)
ValE11	514	1944	1581	1502, 1470	1373 (70%)
					1355 (30%)
TyrE11	514	1940	1581	1502, 1470	1373 (86%)
					1356 (14%)

[a] Data from ref *31*. [b] The RR spectra were decomposed using peak fitting software from Grams spectra. The relative intensity of each band was calculated by the ratio of their height to the total relative height. [c] Not determined.

This GlnE7 orientation in the PheB10Val mutant can generate the structure involving H-bonding interaction with the water molecule as observed in the RR study. Changes in GlnE7 orientation were also predicted for PheB10Leu (Figure 10, right panel) and, to a lesser extent, for the E11 mutants (not shown). Similar variations in distal structures can be invoked for the HbI−H_2S mutant derivatives, altering in turn sulfide reactivity within these proteins samples, as judged by their responses in heme reduction.

Reduction of the Heme Active Center by Hydrogen Sulfide. Figure 11 and Table 2 show that reduction of the HbI ferric iron center upon reaction with H_2S is controlled by the residues at the distal active site as judged by the increase in the intensity of the oxidation state marker band ν_4 at 1356 cm^{-1} and the ν_{Fe-His} mode at 219 cm^{-1}, which are characteristic of deoxy-like species. The relative intensity of the 1356 cm^{-1} band can be obtained for each mutant by calculating the ratio of its height to the total relative height of both the ν_4 1356 and 1372 cm^{-1} peaks. Accordingly, the faster reduction reactions for the PheB10Val, GlnE7His, and PheB10Leu mutants are evidenced by the 68 and 47% contributions of the 1356 cm^{-1} band. Likewise, although to a lesser extent, reaction of PheE11Val, PheB10Tyr, PheE11Tyr, and rHbI with H_2S produced rapid reduction of the ferric iron with 30, 20, 14, and 13% contributions of the 1356 cm^{-1} band, respectively. While no immediate reduction of the ferric iron atom was observed for the PheE7Val mutant, a small contribution of the ν_4 band at 1356 cm^{-1} was detected as a function of time, indicating a very slow electron transfer reaction for this variant. The dependence of the heme reduction process on distal side residues can be explained in principle by the strength and directionality of the hydrogen bond between the E7 residue and the bound H_2S. In the case of GlnE7Val, the lack of proton acceptor groups in the proximity of the bound ligand retards substantially the reduction of the heme iron induced by H_2S. In the GlnE7His variant, the N atom of the imidazole side chain forms a stronger hydrogen bond (when compared to rHbI) with the bound H_2S, thus inducing a faster electron transfer to the ferric iron. For the PheB10Val and PheB10Leu mutants, movement of the GlnE7 carbonyl group toward the ferric iron may place this side chain in a new orientation to form a more stable and stronger H-bond with H_2S, accelerating in turn the reduction and consequent formation of the unbound deoxy species, as judged by the rapid increase in the intensity of the Fe−His mode (Figure 11, right panel). A similar mechanism can be invoked for the E11 mutations. However, mutation of PheE11 to either Val or Tyr changes the direction of the GlnE7 carbonyl group so that

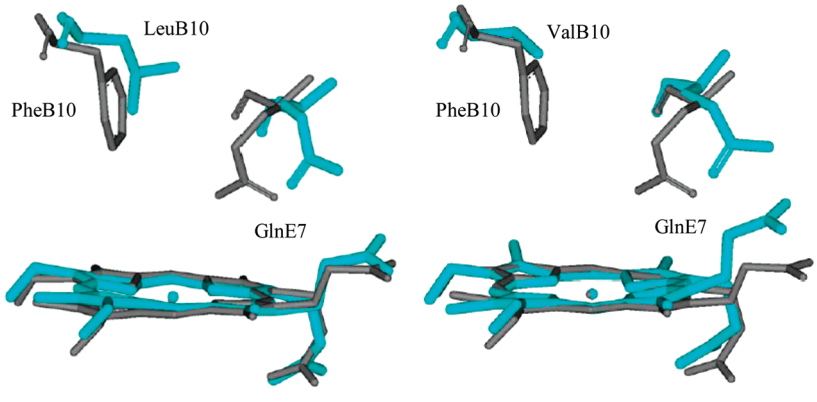

FIGURE 10: Representations of the B10 mutated residue and GlnE7 in the distal heme of HbI (gray) and the PheB10Leu mutant (blue) are shown at the left, while those for HbI (gray) and the PheB10Val mutant (blue) are displayed at the right.

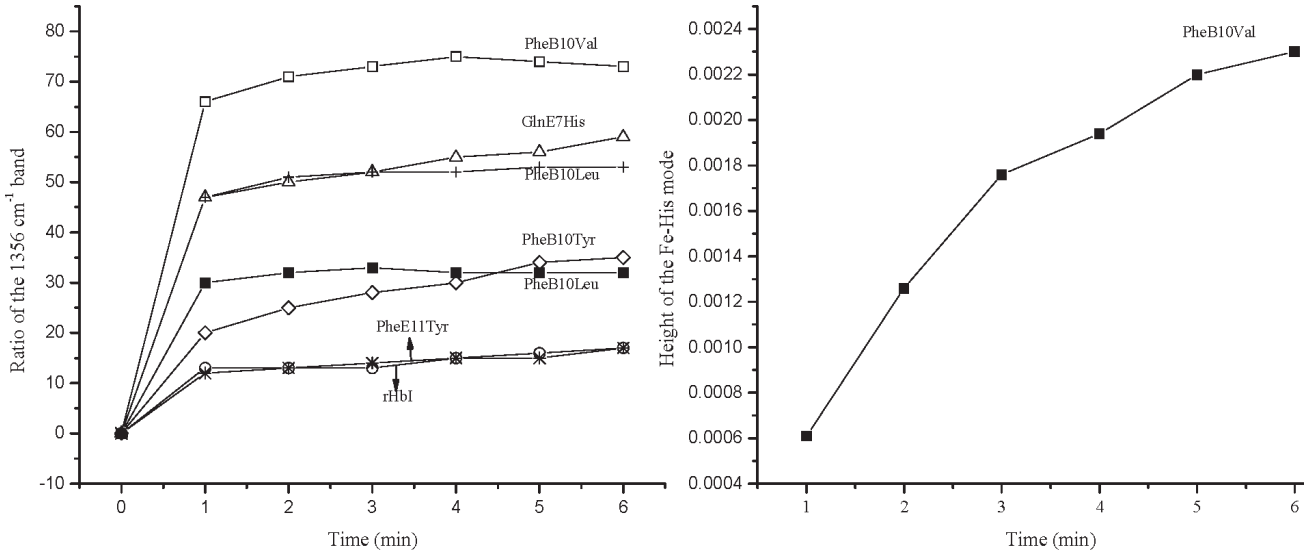

FIGURE 11: Relative intensity of the 1356 cm^{-1} band as a function of time for various HbI mutants (left panel). The intensities were obtained by calculating the ratio of its height to the total relative height of both the ν_4 1356 and the 1372 cm^{-1} peaks. On the right, the peak of the Fe−His mode for the PheB10Val mutant vs time is shown.

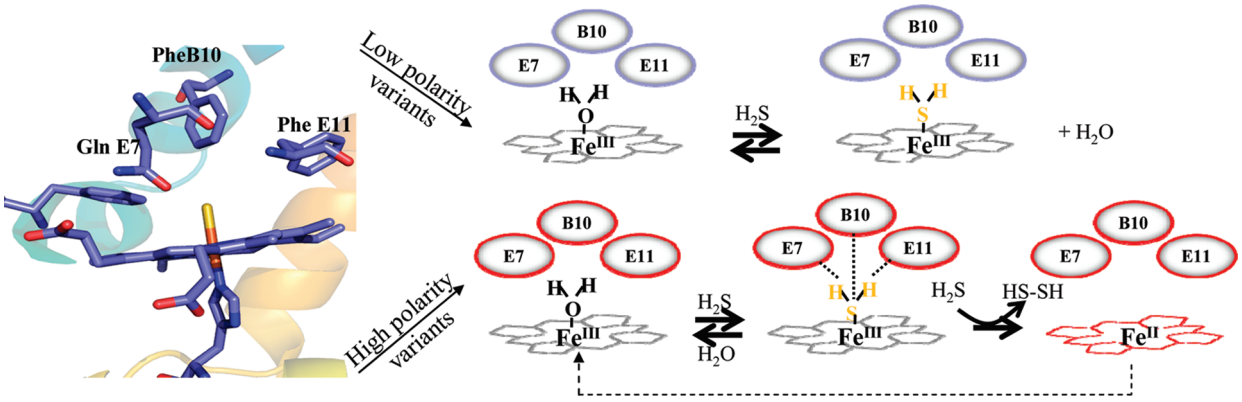

FIGURE 12: Hypothesized reactions of H_2S with hemeproteins deduced from the results of the HbI site-directed mutants.

the hydrogen bond becomes weaker than that in the B10 mutants but stronger than that in the recombinant wild-type protein.

Factor Affecting the Reactivity of Hydrogen Sulfide with Hemeproteins. The results obtained with the HbI site-directed mutants indicate that interactions of H_2S with hemeproteins are controlled by the following factors: (i) accessibility of H_2S to the heme cavity, (ii) H_2S concentration, (iii) polarity of the distal environment surrounding the bound H_2S, and (iv) stereo orientation of the distal side residues. At the limit of complex formation (3−10-fold H_2S molar excess), hemeproteins with a rather open distal pocket will react with H_2S, readily forming the heme−H_2S complex, as judged by the H_2S bimolecular binding reactions. Sulfide release is then dictated by two competing processes involving simple dissociation of H_2S from the ferric adduct and heme iron reduction induced by H_2S itself. The complex behavior of H_2S dissociation kinetics can be related to these species. The electron transfer process is greatly enhanced at high H_2S concentrations and in those variants having proton acceptor groups near the bound H_2S. For instance, in GlnE7His, PheB10Val, and PheB10Leu, the reduction could take place without large excesses of H_2S (≤10-fold molar excess), as evidenced by the immediate appearance of the ν_4 mode in their RR spectra. In fact, the spectral changes associated with dissociation of H_2S from the GlnE7His mutant, which were taken at the limit of complex formation, show the generation of an oxy-like species, suggesting rapid reduction of the heme and formation of this derivative.

Scheme 1: Reaction Proposed for the Interaction of H_2S with Low-Polarity Heme Pocket Environments

$$HemeFe^{III} - H_2O + H_2S \leftrightarrow HemeFe^{III} - H_2S + H_2O$$

On these bases, we proposed that interaction of H_2S with hemeproteins can be generalized by the reactions schematized in Figure 12. On the limit of complex formation, proteins with a low-polarity distal environment in the vicinity of the iron will react with H_2S according to Scheme 1.

In this context, these proteins will bind H_2S and sulfide release is then dictated by simple dissociation of H_2S from the ferric adducts without inducing significant heme reduction. Furthermore, heme pockets with a distal polar environment in which their residues are not oriented to form strong H-bonding interactions with H_2S can follow the same reaction. In contrast, hemeproteins with polar side chains showing stereo orientations favorable for formation of strong H-bonding interactions with the bound ligand can stimulate the reduction process under the same conditions as shown in Scheme 2. In these hemeproteins, the H-bonding interaction between the polar residues and the bound H_2S can induce rapid deprotonation of H_2S, stimulating in turn

Scheme 2: Reaction Proposed for the Interaction of H_2S with High-Polarity Heme Pocket Environments

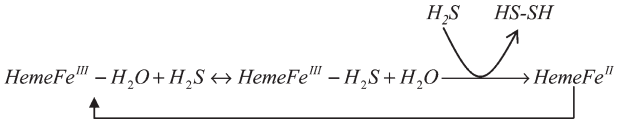

the formation of a $Fe^{II}-SH^{\bullet}$ radical intermediate by one electron transfer from the $Fe^{III}-SH^{-}$ moiety. In the presence of a slight excess of ligand, H_2S can react with the $Fe^{II}-SH^{\bullet}$ radical intermediate, producing in turn the final deoxy heme Fe^{II} and disulfide species.

This reduction reaction is supported by the observation that interaction of H_2S with other hemeproteins, such as cytochrome *c* oxidase (*8*, *10*) and flavocytochrome *c* sulfide dehydrogenase (*41*), induces heme reduction and generates $SH^{\bullet}$ radical intermediates and final disulfides or elemental sulfur at low and high H_2S concentrations, respectively. Reduction of the heme iron center by several organic thiols with the concomitant generation of $SH^{\bullet}$ radical intermediates and final disulfide compounds has also been suggested to occur in myoglobin (*42*). Moreover, oxidation of the reduced Mb by the disulfide products was also observed in that work.

We therefore suggest that these disulfides or hydrogen persulfide species (H_2S_2) can in principle oxidize the reduced heme, reconverting the deoxy species to the active metaquo form of the protein. Alternatively, spontaneous autoxidation of the ferrous heme can occur, resulting in the formation of the functional ferric protein as indicated in Scheme 2. As with other hemeproteins (*24*), this autoxidation process should be influenced by the properties of each mutant.

Thus, for wtHbI, the flexibility of GlnE7 allows H_2S to bind rapidly to the ferric heme. Stabilization of the bound H_2S through H-bonding interaction with GlnE7 can in turn induce some heme reduction and H_2S delivery as a function of H_2S concentration. The fact that the X-ray structure of HbI indicates that its heme group is more exposed to the solvent than in HbII (*21*) suggests that heme oxidation of the ferrous iron can occur, reconverting the deoxy species to the metaquo form of the protein as H_2S is being consumed.

In the case of Mb, HisE7 lies close to the active center (*43*) and its reaction with a small excess of H_2S induces not only reduction of the heme but also sulfmyoglobin formation (*11*, *12*). This further indicates that the proper orientation of the distal residues is not only important for heme reduction induced by H_2S but also crucial for sulfhemeprotein formation. Consistent with this argument is the fact that under certain conditions, H_2S provokes reduction of the ferric heme a_3 in cytochrome *c* oxidase, which is characterized by a very polar distal heme site involving the Cu_B center and a Tyr at position 244, without an apparent formation of sulfheme species (*9*).

Interestingly, the interaction of human neuroglobin (Ngb) with H_2S has been examined recently for the first time by analyzing its binding reaction with the ferric center of this new member of the globin family, which is especially abundant in the brains of mammals (*14*). It was found in this study that H_2S association, using a 400-fold sulfide molar excess, followed biphasic behavior with a fast process being concentration-dependent and a slower one being independent of H_2S concentration. The rapid reaction was ascribed to the bimolecular binding of H_2S, while the slowest was not attributed to any particular process. On the basis of the structural properties of Ngb (*44*) and factors affecting H_2S reactivity presented here, we suggest that heme iron reduction should be considered for the slow process observed in the H_2S binding reaction with this hemeprotein. The distal heme cavity of Ngb is characterized by the presence of a HisE7 coordinated to the heme iron in the absence of exogenous ligand (*45*). Upon exogenous ligation, HisE7 is detached from the iron but still near the bound ligand (*46*). Hence, reaction of a large excess of H_2S with Ngb can also induce iron reduction due to the peculiar HisE7 orientation, and it should be contemplated when analyzing the interaction of H_2S with this hemeprotein.

Although reduction of hemeproteins by H_2S has been observed before, the dependence of this process on the polarity of the distal site environment should be taken into account when considering interaction of hemeproteins as well as metalloproteins with H_2S. This can explain, in principle, the different responses that H_2S exerts on hemeproteins and in different tissues and how they can influence sulfide biological activities within cells.

ACKNOWLEDGMENT

We thank graduate and undergraduate students Laura Granell, Abner Nieves, and Frances Marie Pietri for their technical assistance during the work.

REFERENCES

1. Reiffenstein, R. J., Hulbert, W. C., and Roth, S. H. (1992) Toxicology of Hydrogen Sulfide. *Annu. Rev. Pharmacol. Toxicol.,* 109–134.
2. Li, L., and Moore, P. (2008) Putative biological roles of hydrogen sulfide in health and disease: A breath of not so fresh air?. *Trends Pharmacol. Sci. 29*, 84–90.
3. Chen, C. Q., Xin, H., and Zhu, Y. Z. (2007) Hydrogen sulfide: Third gaseous transmitter, but with great pharmacological potential. *Acta Pharmacol. Sin. 28*, 1709–1716.
4. Li, L., and Moore, P. K. (2007) An overview of the biological significance of endogenous gases: New roles for old molecules. *Biochem. Soc. Trans. 35*, 1138–1141.
5. Łowicka, E., and Bełtowski, J. (2007) Hydrogen sulfide (H_2S): The third gas of interest for pharmacologists. *Pharmacol. Rep. 59*, 4–24.
6. Szabó, C. (2007) Hydrogen sulphide and its therapeutic potential. *Nat. Rev. Drug Discovery 6*, 917–935.
7. Blackstone, E., Morrison, M., and Roth, M. B. (2005) H_2S induces a suspended animation-like state in mice. *Science 308*, 518.
8. Nicholls, P., and Kim, J. K. (1981) Oxidation of sulphide by cytochrome *aa3*. *Biochim. Biophys. Acta 637*, 312–320.
9. Nicholls, P., and Kim, J. K. (1982) Sulphide as an inhibitor and electron donor for the cytochrome *c* oxidase system. *Can. J. Biochem. 60*, 613–623.
10. Hill, B. C., Woon, T. C., Nicholls, P., Peterson, J., Greenwood, C., and Thomson, A. J. (1984) Interactions of sulphide and other ligands with cytochrome *c* oxidase. An electron-paramagnetic-resonance study. *Biochem. J. 224*, 591–600.
11. Johnson, E. A. (1970) The reversion to haemoglobin of sulphhaemoglobin and its coordination derivatives. *Biochim. Biophys. Acta 207*, 30–40.
12. Berzofsky, J. A., Peisach, J., and Blumberg, W. E. (1971) Sulfheme proteins. I. Optical and magnetic properties of sulfmyoglobin and its derivatives. *J. Biol. Chem. 246*, 3367–3377.
13. Bailly, X., and Vinogradov, S. (2005) The sulfide binding function of annelid hemoglobins: Relic of an old biosystem?. *J. Inorg. Biochem. 99*, 142–150.
14. Brittain, T., Yosaatmadja, Y., and Henty, K. (2008) The interaction of human neuroglobin with hydrogen sulphide. *IUBMB Life 60* 135–138.
15. Weber, R. E., and Vinogradov, S. N. (2001) Nonvertebrate hemoglobins: Functions and molecular adaptations. *Physiol. Rev. 81*, 569–628.
16. Kraus, D. W., and Wittenberg, J. B. (1990) Hemoglobins of the *Lucina pectinata*/bacteria symbiosis I. *J. Biol. Chem. 265*, 16043–16053.
17. Kraus, D. W., and Wittenberrg, J. B. (1990) Hemoglobins of the *Lucina pectinata*/bacteria symbiosis II. *J. Biol. Chem. 265*, 16054–16059.

18. Rizzi, M., Wittenberg, J. B., Coda, A., Ascenzi, P., and Bolognesi, M. (1996) Structural bases for sulfide recognition in *Lucina pectinata* hemoglobin I. *J. Mol. Biol. 258*, 1–5.
19. Pietri, R., Granell, L., Cruz, A., De Jesús, W., Lewis, A., Leon, R., Cadilla, C. L., and Garriga, J. L. (2005) Tyrosine B10 and heme-ligand interactions of *Lucina pectinata* hemoglobin II: Control of heme reactivity. *Biochim. Biophys. Acta 1747*, 195–203.
20. De Jesús-Bonilla, W., Cruz, A., Lewis, A., Cerda, J., Bacelo, D. E., Cadilla, C. L., and López-Garriga, J. (2006) Hydrogen-bonding conformations of tyrosine B10 tailor the hemeprotein reactivity of ferryl species. *J. Biol. Inorg. Chem. 11*, 334–342.
21. Gavira, J. A., Camara-Artigas, A., De Jesús-Bonilla, W., López-Garriga, J., Lewis, A., Pietri, R., Yeh, S.-R., Cadilla, C. L., and García-Ruiz, J. M. (2008) Structure and Ligand Selection of Hemoglobin II from *Lucina pectinata*. *J. Biol. Chem. 283*, 9414–9423.
22. Nguyen, B. D., Zhao, X., Vyas, K., La Mar, G. N., Lile, R. A., Brucker, E. A., Phillips, J. N., Olson, J. S., and Wittenberg, J. B. (1998) Solution and crystal structures of a sperm whale myoglobin triple mutant that mimics the sulfide-binding hemoglobin from *Lucina pectinata*. *J. Biol. Chem. 273*, 9517–9526.
23. Pietri, R., León, R. G., Kiger, L., Marden, M. C., Granell, L. B., Cadilla, C. L., and López-Garriga, J. (2006) Hemoglobin I from *Lucina pectinata*: A model for distal heme-ligand control. *Biochim. Biophys. Acta 1764*, 758–765.
24. Springer, B. A., Sligar, S. G., Olson, J. S., and Phillips, G. N.Jr. (1994) Mechanisms of ligand recognition in myoglobin. *Chem. Rev. 94*, 699–714.
25. Draghi, F., Miele, A. E., Travaglini-Allocatelli, C., Vallone, B., Brunori, M., Gibson, Q. H., and Olson, J. S. (2002) Controlling ligand binding in myoglobin by mutagenesis. *J. Biol. Chem. 277*, 7509–7519.
26. Bikiel, D. E., Boechi, L., Capece, L., Crespo, A., De Biase, P. M., Di Lella, S., González Lebrero, M. C., Martí, M. A., Nadra, A. D., Perissinotti, L. L., Scherlis, D. A., and Estrin, D. A. (2006) Modeling heme proteins using atomistic simulations. *Phys. Chem. Chem. Phys. 8*, 5611–5628.
27. Egawa, T., and Yeh, S. R. (2005) Structural and functional properties of hemoglobins from unicellular organisms as revealed by resonance Raman spectroscopy. *J. Inorg. Biochem. 99*, 72–96.
28. León, R. G., Munier-Lehmann, H., Barzu, O., Baudin-Creuza, V., Pietri, R., López-Garriga, J., and Cadilla, C. L. (2004) High-level production of recombinant sulfide-reactive hemoglobin I from *Lucina pectinata* in *Escherichia coli*. High yields of fully functional holoprotein synthesis in the BLi5 E. coli strain. *Protein Expression Purif. 38*, 184–195.
29. Kiger, L., Poyart, C., and Marden, M. C. (1993) Oxygen and CO binding to triply NO and asymmetric NO/CO hemoglobin hybrids. *Biophys. J. 65*, 1050–1058.
30. Collazo, E., Pietri, R., De Jesús, W., Ramos, C., Del Toro, A., Leon, R., Cadilla, C. L., and Lopez-Garriga, J. (2004) Functional Characterization of the Purified Holo form of Hemoglobin I from *Lucina pectinata* Over-Expressed in *Escherichia coli*. *Protein J. 23*, 239–245.
31. University of California, San Francisco. Available at http://www.amber.ucsf.edu.
32. Canutescu, A. A., Shelenkov, A. A., and Dunbrack, R. L.Jr. (2003) A graph-theory algorithm for rapid protein side-chain prediction. *Protein Sci. 12*, 2001–2014.
33. Cornell, W. D., Cieplak, P., Bayly, C. I., Gould, I. R., Merz, K. M., Ferguson, D. M., Spellmeyer, D. C., Fox, T., Caldwell, J. W., and Kollman, P. A. (1995) A 2nd generation force-field for the simulation of proteins, nucleicacids, and organic-molecules. *J. Am. Chem. Soc. 117*, 5179–5197.
34. Jorgensen, W. L., Chandrasekhar, J., Madura, J. D., Impey, R. W., and Klein, M. L. (1983) Comparison of simple potential functions for simulating liquid water. *J. Chem. Phys. 79*, 926–935.
35. Fernandez-Alberti, S., Bacelo, D. E., Binning, R. C.Jr., Echave, J., Chergui, M., and Lopez-Garriga, J. (2006) Sulfide-binding hemoglobins: Effects of mutations on the active-site flexibility. *Biophys. J. 91*, 1698–1709.
36. Berendsen, H. J. C., Postma, J. P. M., Vangunsteren, W. F., Dinola, A., and Haak, J. R. (1984) Molecular-dynamics with coupling to an external bath. *J. Chem. Phys. 81*, 3684–3690.
37. Zamyatin, A. A. (1972) Protein volume in solution. *Prog. Biophys. Mol. Biol. 24*, 107–123.
38. Cerda, J., Echevarría, Y., Morales, E., and López-Garriga, J. (1999) Resonance Raman studies of the heme-ligand active site of hemoglobin I from *Lucina pectinata*. *Biospectroscopy 5*, 289–301.
39. Dou, Y., Maillett, D. H., Eich, R. F., and Olson, J. S. (2002) Myoglobin as a model system for designing heme protein based blood substitutes. *Biophys. Chem. 10*, 127–148.
40. Morikis, D., Champion, P. M., Springer, B. A., Egebey, K. D., and Sligar, S. G. (1990) Resonance Raman studies of iron spin and axial coordination in distal pocket mutants of ferric myoglobin. *J. Biol. Chem. 265*, 12143–12145.
41. Steudel, R. (1996) Mechanism for the formation of elemental sulfur from aqueous sulfide in chemical and microbiological desulfurization processes. *Ind. Eng. Chem. Res. 35*, 1417–1423.
42. Romero, F. J., Ordoñez, I., Arduini, A., and Cadenas, E. (1992) The reactivity of thiols and disulfides with different redox state of myoglobin. Redox and addition reactions and formation of thiyl radical intermediates. *J. Biol. Chem. 267*, 1680–1688.
43. Kundu, S., Blouin, G. C., Premer, S. A., Sarah, G., Olson, J. S., and Hargrove, M. S. (2004) Tyrosine B10 inhibits stabilization of bound carbon monoxide and oxygen in soybean leghemoglobin. *Biochemistry 43*, 6241–6252.
44. Pesce, A., Dewilde, S., Nardini, M., Moens, L., Ascenzi, P., Hankeln, T., Burmester, T., and Bolognesi, M. (2003) Human brain neuroglobin structure reveals a distinct mode of controlling oxygen affinity. *Structure 11*, 1087–1095.
45. Nienhaus, K., Kriegl, J. M., and Nienhaus, G. U. (2004) Structural dynamics in the active site of murine neuroglobin and its effects on ligand binding. *J. Biol. Chem. 279*, 22944–22952.
46. Ishikawa, H., Finkelstein, I. J., Kim, S., Kwak, K. Chung, J. K., Wakasugi, K., Massari, A. M., and Fayer, M. D. (2007) Neuroglobin dynamics observed with ultrafast 2D-IR vibrational echo spectroscopy. *Proc. Natl. Acad. Sci. U.S.A. 104*, 16116–16121.